Analysis of nuclear fission properties with the Langevin approach in Fourier shape parametrization

Li-Le Liu,[1,*] Yong-Jing Chen,[1] Xi-Zhen Wu,[1,†] Zhu-Xia Li,[1] Zhi-Gang Ge,[1] and Krzysztof Pomorski[2,‡]
[1]*China Nuclear Data Center, China Institute of Atomic Energy, Beijing 102413, China*
[2]*Institute of Physics, Maria Curie Skłodowska University, 20-031 Lublin, Poland*

(Received 2 February 2021; accepted 16 March 2021; published 1 April 2021)

The Langevin approach is extendedly applied to study the dynamical process of nuclear fission within the Fourier shape parametrization, where the potential energy is calculated with the macroscopic-microscopic model based on the Lublin-Strasbourg drop model and the Yukawa-folded potential. The fragment mass distribution and the total kinetic energy as a function of heavy fragment mass in 14 MeV $n + {}^{235}$U fission are calculated and compared with the evaluated data from ENDF/B-VIII.0 and the experimental data. It is found that the Wall model for the friction tensor is available to describe both of the mass distribution and the total kinetic energy (TKE) distribution in the nuclear fission within the present model. In addition, the mass distributions and the TKE distributions in 14 MeV $n + {}^{233,236,238}$U and ^{239}Pu fission are well described. Furthermore, the behavior of the correlation of the distance between the centers of mass of two fragments with the heavy fragment mass at the scission point is found to be consistent with that of the TKE distribution where the shortest R_{12} locates around $A_h = 135$ which is due to the influence of the shell effects.

DOI: 10.1103/PhysRevC.103.044601

I. INTRODUCTION

The fission process evolves slowly from a compact nucleus towards two separated fragments, which involves a large-scale and highly dissipative collective motion coupled with internal degrees of freedom. Despite great progress in the study of nuclear fission within the framework of microscopic or macroscopic approaches in recent years [1–20], the dynamical process towards the scission point is still not completely understood, and the knowledge about the scission configuration is quite lacking.

In the theoretical description of nuclear fission, the parametrization of nuclear shape and the potential energy surface are generally important ingredients, which have a significant influence on the predictive power of the dynamical model. Up to now, several shape parametrizations have been developed and applied in the description of nuclear fission [21], including the two-center shell model (TCSM) [12–14,18,20,22,23]. We have used the three-dimensional Langevin approach with TCSM plus a constraint on the shape of the heavy peak fragment ($N = 82$ shell closure) to study the fission dynamics for uranium and plutonium isotopes at low excitation energies and the fragment mass distributions are well reproduced [20]. Recently the Fourier shape parametrization has been introduced in Ref. [24], which has the virtue of convenience to handle due to its analytical expression and rapidly converging. The calculation time needed is much shorter compared with the TCSM calculations.

This method can generate a rich variety of shapes with only three free shape parameters. In addition, the Fourier parametrization was used to construct a simple three-dimensional (3D) collective model obtained by using the Born-Oppenheimer approximation in which the nuclear dissipation is only partially taken into account [11], and the main characteristics of fission fragment mass distributions were well reproduced for even-even Pt to Ra isotopes at the lower temperature, where the potential energy surface is evaluated within the macroscopic-microscopic approach based on the Lublin-Strasbourg drop (LSD) model [25] and the Yukawa-folded single-particle potential [26,27]. In this work, the potential energy surface within the Fourier shape parametrization is extendedly applied in studying the dynamical process of nuclear fission using a 3D Langevin approach. The fragment mass and the total kinetic energy distributions for 14 MeV $n + {}^{233,235,236,238}$U and ^{239}Pu fission as well as the mass-energy correction of fragments in 14 MeV $n + {}^{235}$U fission are calculated, which verify the applicability and reliability of the model during the dynamical calculation. Furthermore, we also study the correlation between the deformation parameters at the scission point, which deepens the understanding of the dynamical process of nuclear fission.

This paper is organized as follows. A detailed introduction of the model is presented in Sec. II. The calculated fragment mass distributions and total kinetic energy distributions as well as the configuration at the scission point are shown in Sec. III. A summary of the present work and prospects are presented in Sec. IV.

II. METHODS

A. The Fourier shape parametrization

The nuclear shapes involved in the fission process cover a rich variety of shapes including not only the mononuclear shapes but also the dinuclear shapes, and several powerful

*liulile401@163.com
†lizwux9@ciae.ac.cn
‡pomorski@kft.umcs.lublin.pl

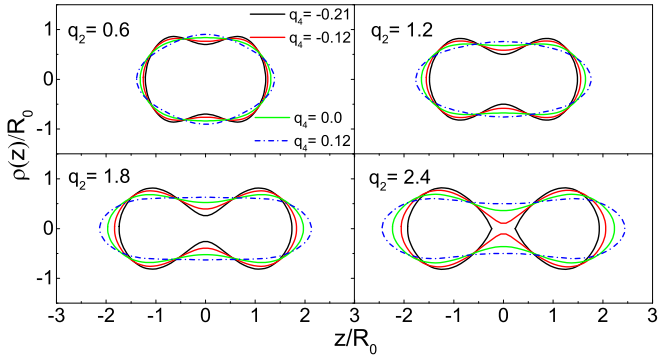

FIG. 1. The nuclear shapes described within the Fourier shape parametrization ($q_3 = 0.0$).

shape parametrizations have been developed in the past. In the present work, the surface of the fissioning nucleus is described by using the recently proposed Fourier shape parametrization [24] which could be rapidly converging and analytical. For an axially symmetric nucleus, the nuclear surface can be expanded in a Fourier series in cylindrical coordinate as follows:

$$\frac{\rho_s^2(z)}{R_0^2} = \sum_{n=1}^{\infty}\left[a_{2n}\cos\left(\frac{(2n-1)\pi}{2}\frac{z-z_{sh}}{z_0}\right) + a_{2n+1}\sin\left(\frac{2n\pi}{2}\frac{z-z_{sh}}{z_0}\right)\right], \tag{1}$$

where $\rho_s(z)$ is the distance of the point at the surface to the symmetric axis (z axis) and R_0 denotes the radius of the spherical shape having the same volume, i.e., $R_0 = 1.2A^{1/3}$ fm. The left end and right end are located at $z_{\min} = z_{sh} - z_0$ and $z_{\max} = z_{sh} + z_0$, respectively. z_0 is the half of extension of the shape along the symmetry axis, which can be obtained from the volume conservation, and z_{sh} is determined by imposing the condition that the center of mass of the nuclear shape is located at the origin of the coordinate system. The Fourier parametrization is very rapidly converging and only the first five terms, i.e., $a_2, \ldots, a_6$, are needed with enough accuracy. In the description of the fission process, the parameters a_n are usually transformed to the deformation parameters q_n in the following way:

$$\begin{aligned} q_2 &= a_2^{(0)}/a_2 - a_2/a_2^{(0)}, \\ q_3 &= a_3, \\ q_4 &= a_4 + \sqrt{(q_2/9)^2 + \left(a_4^{(0)}\right)^2}, \\ q_5 &= a_5 - (q_2 - 2)a_3/10, \\ q_6 &= a_6 - \sqrt{(q_2/100)^2 + \left(a_6^{(0)}\right)^2}, \end{aligned} \tag{2}$$

where the $a_n^{(0)}$ stands for values of the Fourier coefficients for the spherical shape. The higher-order coordinates q_5 and q_6 are generally set to be zero within the accuracy of the present approach. Figure 1 shows a series of nuclear shapes described within the Fourier parametrization, where different values of q_2 and q_4 are taken and q_3 is set to be zero (i.e., left-right mass-symmetric). It indicates that the set of q_i has explicit physical meaning in describing the shape of the fissioning nucleus, i.e., q_2 denotes the elongation of the nucleus and q_4 is the neck parameter, and q_3 is the left-right asymmetry parameter. Therefore, the dynamical process of nuclear fission can be described in the three-dimensional deformation space $\{q_2, q_3, q_4\}$ within the Fourier shape parametrization. It should be noted that the nonaxiallity is not taken into account in the present work, since it plays an important role only in the vicinity of the ground state and the first saddle point [24].

B. The potential energy, inertia tensor, and friction tensor

The potential energy, inertia tensor, and friction tensor, which are dependent on the nuclear deformation, are the basic ingredients of the Langevin equation. In this work, the macroscopic-microscopic approach is adopted to calculate the potential energy of the fissioning system, which is represented by the sum of the liquid drop energy and the microscopic correction energy for the same nuclear shape. The macroscopic energy is evaluated with the LSD model [25], with the deformation-dependent terms being taken into account, which includes the surface energy, the Coulomb energy, the curvature energy, and congruence energy. For the microscopic energy, we calculate the shell correction energy using the Strutinsky method [28] and the pairing correction is calculated with the Bardeen-Cooper-Schrieffer (BCS) method [29,30] based on the single-particle levels obtained from the Yukawa-folded mean-field potential [26,27]. Also, the temperature dependence of the microscopic energy is introduced to describe the fissioning system at certain excitation energy [31]:

$$\begin{aligned} V(q,T) &= V_{\rm mac}(q) + V_{\rm mic}(q, T=0)\phi(T), \\ \phi(T) &= \exp(-aT^2/E_d), \end{aligned} \tag{3}$$

where a is the level density parameter of the compound nucleus and E_d represents the damping parameter of the microscopic correction energy. In the present work, we use the constant value $A_{CN}/10$ MeV^{-1} for the level density parameter a, as it is found that the calculated mass distributions are not sensitive depending on the parameter a in a reasonable range [20]. And the shell damping parameter E_d is taken to be 60 MeV for the even-even fissioning system which is similar to Ref. [32] and 50 MeV for the odd-A fissioning system.

The calculated potential energy surface of ^{236}U at zero temperature relative to the corresponding spherical LSD energy as a function of elongation q_2 and mass asymmetry q_3 is shown in Fig. 2, in which the energy is minimized with respect to q_4. It can be clearly seen that the ground state locates around $q_2 \approx 0.3$ and $q_3 \approx 0.0$, and the mass-symmetric saddle lays a few MeV higher than the mass-asymmetric saddle after crossing the first saddle point where the optimal fission path walks along the asymmetric fission channel.

The inertia tensor is calculated within the macroscopic hydrodynamic method, where the nucleus is assumed to be an incompressible and irrotational liquid drop. The Werner-Wheeler approximation [33] is adopted to calculate the inertia

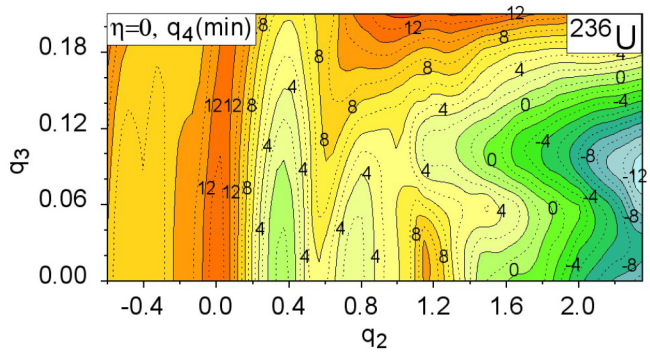

FIG. 2. The deformation energy on the (q_2, q_3) plane of ^{236}U minimized with respect to q_4. Only axial shapes ($\eta = 0$) are taken here into account.

tensor which is expressed in the following form:

$$m_{ij}(q) = \pi \rho_m \int_{z_{\min}}^{z_{\max}} \rho_s^2(z,q)(A_i A_j + \frac{1}{8}\rho_s^2(z,q)A_i' A_j')dz, \quad (4)$$

$$A_i = \frac{1}{\rho_s^2(z,q)} \frac{\partial}{\partial q_i} \int_z^{z_{\max}} \rho_s^2(z',q)dz', \quad (5)$$

where ρ_m denotes the mass density, and A_i' is the differentiation of A_i with respect to z. In the expression of A_i, the integration is from z to the right end $z_{\max}$ for the right part and from the left end $z_{\min}$ to z for the left part, respectively.

The friction tensor is calculated within the one-body Wall model [34–37], in which the corresponding energy dissipation arises from the collision of the inner nucleons with the nuclear surface, which is written as follows:

$$\gamma_{ij}^{\text{Wall}}(q) = \frac{1}{2}\pi \rho_m \overline{\upsilon} \int_{z_{\min}}^{z_{\max}} dz \frac{\partial \rho_s^2}{\partial q_i}\frac{\partial \rho_s^2}{\partial q_j}\left[\rho_s^2 + \frac{1}{4}\left(\frac{\partial \rho_s^2}{\partial z}\right)^2\right]^{-1/2}, \quad (6)$$

where $\overline{\upsilon}$ is the average velocity of inner nucleons and related to the Fermi velocity as $\overline{\upsilon} = \frac{3}{4}\upsilon_f$.

C. The Langevin approach

In the present work, the dynamics of the fission process is described within the Langevin approach, in which the evolution of the collective coordinates is viewed as the motion of Brownian particles that interact stochastically with the inner nucleons. The coupled Langevin equation describing the evolution of the collective coordinates and the conjugate momenta have the following form:

$$\frac{dq_i}{dt} = (m^{-1})_{ij}p_j,$$
$$\frac{dp_i}{dt} = -\frac{\partial V}{\partial q_i} - \frac{1}{2}\frac{\partial (m^{-1})_{jk}}{\partial q_i}p_j p_k - \gamma_{ij}(m^{-1})_{jk}p_k + g_{ij}\Gamma_j(t), \quad (7)$$

where the collective coordinates $\{q_i\}$ represent $\{q_2, q_3, q_4\}$ within the Fourier shape parametrization, and p_i is the generalized momentum conjugate to q_i. The summation convention for repeated indices is taken in this paper. The first term represents the conservative force, in which we use the differentiation of potential energy V with respect to q_i instead of the free energy $F = V - aT^2$, since the level density parameter a is taken to be a constant in this work. The m_{ij} is the inertia tensor and its inverse matrix denotes $(m^{-1})_{ij}$. γ_{ij} is the friction tensor. The last term $g_{ij}\Gamma_j(t)$ is the random force, in which the normalized random force $\Gamma_j(t)$ is assumed to be white noise and obtained by using a Gaussian random number generator, and g_{ij} is the strength of the random force, which is calculated according to the fluctuation-dissipation theorem

$$g_{ik}g_{jk} = \gamma_{ij}T^*, \quad (8)$$

T^* is the effective nuclear temperature, in which the quantum effect is taken into account for nuclear fission at low excitation energy. It is expressed as follows [38,39]:

$$T^* = \frac{\hbar\varpi}{2}\coth\frac{\hbar\varpi}{2T}, \quad (9)$$

where T is the general nuclear temperature, and ϖ is the local frequency of the collective motion. The minimum value of $\hbar\varpi$ is generally given by the zero-point energy. In the present work, we adopt the value $\hbar\varpi = 2$ MeV suggested in Ref. [13]. The temperature T is calculated by the Fermi gas model: $E_{\text{int}} = aT^2$. E_{int} is the intrinsic excitation energy of the compound nucleus and calculated at each time step as follows:

$$E_{\text{int}}(q) = E^* - \tfrac{1}{2}(m^{-1})_{ij}p_i p_j - V(q, T = 0), \quad (10)$$

E^* is the total initial excitation energy of the fissioning nucleus. In the present work, the particle emission along the Langevin trajectory is not taken into account, which will be studied in the future work.

The above Langevin equation is solved by the second order Runge-Kutta numerical method, and the potential energy, inertia tensor, and friction tensor at each time step $t = n\Delta t$ are obtained by the parabola interpolation based on the prepared meshes to save computation time. The mesh values $\{q_2, q_3, q_4\}$ are taken to be

$$q_2 = -0.6(0.05)2.9,$$
$$q_3 = -0.22(0.02)0.22,$$
$$q_4 = -0.3(0.015)0.195.$$

The time step Δt is taken to be 0.9 fm/c. The initial positions of the Langevin trajectories are taken to be beyond the ground state $\{q_2 = 0.3, q_3 = 0.0, q_4 = -0.16\}$, and the initial momenta are simply assumed to be zero. In principle, the initial values should be taken from a distribution defined by the starting temperature. The calculation of the Langevin trajectory is terminated if it arrives at the scission point or reaches the boundaries of the meshes. In this work, the scission point is determined by a fixed neck radius R_n to be 1.2 fm, which is close to the one (1.0 fm) adopted in Ref. [9]. If the trajectory reaches the scission point, the trajectory is treated as a fission event, and the mass numbers and the total kinetic energy of two fission fragments could be obtained. Within the Fourier parametrization, the fragment mass number for asymmetric fission is determined by all the shape parameters, not only by the mass asymmetry parameter q_3 alone. The total kinetic energy is the sum of the Coulomb repulsion energy between

two fragments and the collective kinetic energy at the scission point. The number of the Langevin trajectories reaches at least 1.0×10^5 per fissioning nucleus in the calculations in this work, which guarantees the enough statistic for the calculation results.

III. CALCULATION RESULTS

A. The fragment mass and TKE distributions in 14 MeV n + ^{235}U fission

In this section, the fragment mass and TKE distributions in 14 MeV $n + {}^{235}$U fission as well as the mass-energy correlation of fission fragments are presented. Figure 3 shows the calculated mass distribution for 14 MeV $n + {}^{235}$U fission and the comparison with the calculated result in Ref. [20] and the evaluated data from ENDF/B-VIII.0 [40]. It can be seen that the calculated result, especially the peak position, is overall consistent with the evaluated data, and similar with the calculated result of Ref. [20], except a little narrower width. It verifies the reliability of the potential energy surface including the saddle point configuration within the Fourier parametrization, which almost determines the fragment mass distribution in low-energy nuclear fission [12]. The result also shows that the Wall formula for the friction tensor is available to well describe the fission fragment mass distribution in the present model calculations, despite the narrower peak width, which will be left to the near future work by introducing the random neck rupture into the Langevin trajectories suggested by Sierk [9]. In addition, it should be noted that the calculation results are for the primary fragments, so the mass distribution obtained is on the right side compared to the evaluated data which is obtained after the prompt neutron emission.

In addition to the fragment mass distribution, we also calculate the total kinetic energy distribution of fission fragments, which is another equally important observable related to nuclear fission. The TKE is the sum of the prescission kinetic energy and the Coulomb energy related to repulsion of the fragments, which is approximately treated as that between two charged point particles located at the centers of mass of

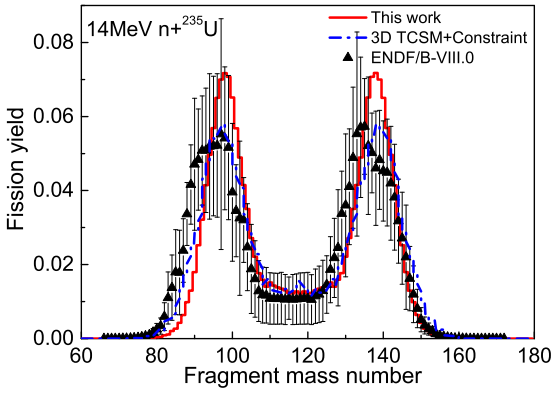

FIG. 3. The calculated fragment mass distribution in 14 MeV $n + {}^{235}$U fission with the present model (red curve) compared with the result calculated with the 3D Langevin approach plus a constraint on the heavy fragment deformation based on the TCSM [20] (blue dashed-dot curve) and the evaluated data from ENDF/B-VIII.0 [40].

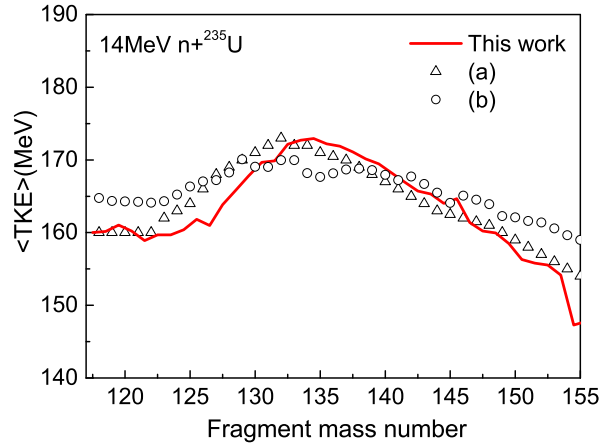

FIG. 4. The calculated TKE as a function of the heavy fragment mass in 14 MeV $n + {}^{235}$U fission compared with the experimental data. The experimental data are taken from (a) [41] and (b) [42], respectively.

two fragments, i.e., $\frac{e^2 Z_1 Z_2}{R_{12}}$. The first term is for sure very small in the presence of the friction force while the Coulomb energy is dominant. Figure 4 shows the calculated TKE in 14 MeV $n + {}^{235}$U fission, along with the experimental data. It can be seen that there is a good agreement between the calculated results and the experimental data both for the symmetric and the asymmetric fission region. In general, the TKE is quite sensitive to the nuclear shapes at the scission point, for the Coulomb repulsion energy between the fragments at the scission point dominates the TKE. The good agreement between the present results and the experimental data indicates that the present model is quite reasonable in the description of the shape at the scission point for the fissioning system studied.

The mass-energy correlation of the fission fragments in 14 MeV $n + {}^{235}$U fission is shown in Fig. 5. It is seen that there is a wide distribution of the TKE for a pair of fragments, due to the different deformations at the fixed mass asymmetry. On the whole, most of the fission events distribute around the heavy fragment mass $A \approx 140$, which corresponds to the peak position of the mass distribution and the largest TKE

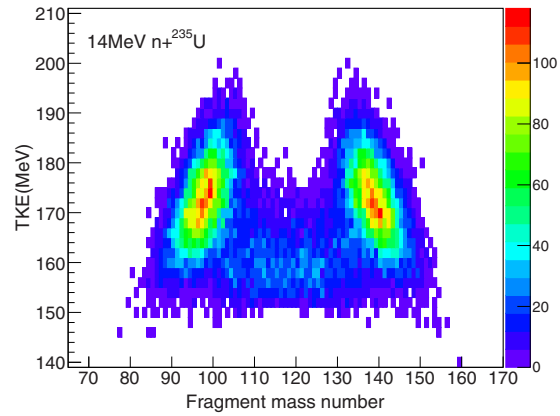

FIG. 5. The calculated mass-energy correlation of the fission fragments in 14 MeV $n + {}^{235}$U fission.

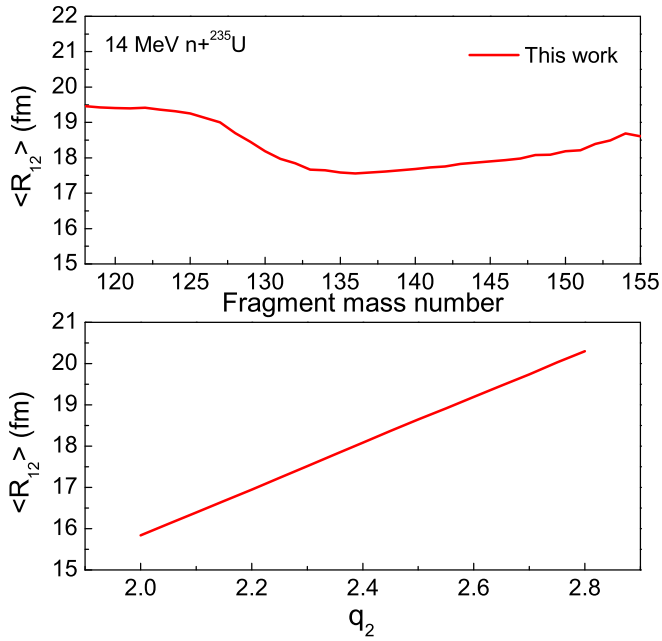

FIG. 6. The correlation between the distance of the mass centers of two fragments R_{12} and the heavy fragment mass at the scission point (upper). the correlation between the R_{12} and the elongation parameter q_2 at the scission point (bottom).

values locate around $A \approx 135$, where the heavy fragment is close to the spherical shape due to the shell effects around the shell closure $Z = 50$ and $N = 82$, which leads to the strongest Coulomb repulsion and the largest TKE as well. In addition, the averaged TKE around the symmetric fission region is about 159 MeV and the lower TKE shows that the symmetric fission channel corresponds to the superlong fission mode. And with the heavy fragment mass number larger than 145 corresponding to the very asymmetric fission case, the TKE value becomes lower than that around the symmetric region, and the neutron number of the corresponding heavy fragment is far from the deformed shell $N = 88$ and therefore the deformation becomes larger.

B. The scission point configuration

The scission point is defined as the terminating point of the Langevin trajectories, which are determined by the dynamical process of nuclear fission. In general, the scission point configuration can provide information about the correlation between the deformation parameters corresponding to different nuclear shapes at the scission point, which helps us to understand the fission mechanism. In this section, we show the correlation of the distance between the mass centers of two complementary fragments R_{12} with the heavy fragment mass at the scission point in Fig. 6. It shows that the R_{12} is much larger around the symmetric mass region, and with the mass asymmetry increasing the R_{12} decreases and then reaches the minimum around $A \approx 135$, for which the fragment shape is close to the spherical shape. When the heavy fragment mass further increases, the R_{12} increases slowly. The overall behavior of the correlation between the R_{12} and the fragment mass

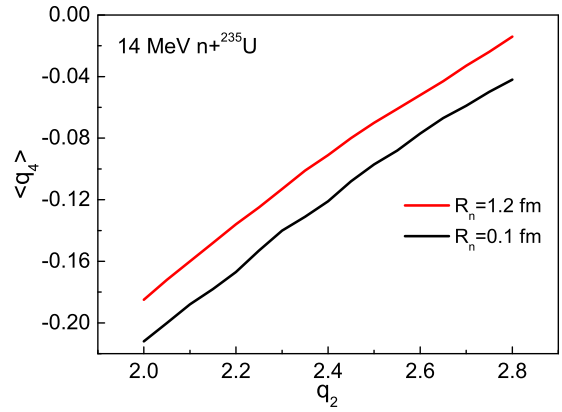

FIG. 7. The correlation between the neck parameter q_4 and the elongation parameter q_2 at the scission point where the neck radius is set to be 1.2 fm (red curve) and 0.1 fm (black curve), respectively.

is consistent with the behavior of the correlation between the TKE and the fragment mass shown in Figs. 4 and 5.

The correlation between R_{12} and the elongation parameter q_2 at the scission point is also obtained from the dynamical calculation and shown at the bottom of Fig. 6. One can see that R_{12} increases linearly with the q_2 at the scission point, which supports that q_2 is suitable to describe the elongation of the system at scission point. Furthermore, the dynamical simulation with the Langevin approach could verify the validity of the collective model obtained using the Born-Oppenheimer approximation [11], where the q_2 direction is related to the slow motion towards fission.

Besides, concerning the correlation of shape parameters, we study the correlation between the neck parameter q_4 and the elongation parameter q_2 at the scission point in Fig. 7, which shows that the averaged q_4 increases nearly linearly with the q_2 at the scission point defined by the fixed neck radius (1.2 fm). And the result of the correlation is compared with that of the case where the scission neck radius R_n is set as 0.1 fm. One can see that the slopes of the two lines are the same but the line for the small neck radius case is shifted downward, and it leads to a too elongated shape and thus a too small TKE when the scission point is defined by a small neck radius. Therefore, in this work, the neck radius at the scission point is defined as 1.2 fm.

C. The calculated fragment mass and the TKE distributions for the more fissioning systems

Within the present model, the fragment mass distributions in 14 MeV $n + {}^{233,236,238}$U and ^{239}Pu fission are calculated as shown in Fig. 8 together with the evaluated data from ENDF/B-VIII.0 and the results in Ref. [20] for $n + {}^{233}$U and ^{239}Pu fission. It can be seen that the agreements between the calculated results and the evaluated data are as good as that shown in Fig. 3, especially in the cases for 14 MeV $n + {}^{233}$U and ^{239}Pu fission, in which the calculated results agree well with the evaluated data and the results in Ref. [20]. As for the calculations in 14 MeV $n + {}^{236,238}$U fission, the peak widths of the mass distributions are narrower and the corresponding

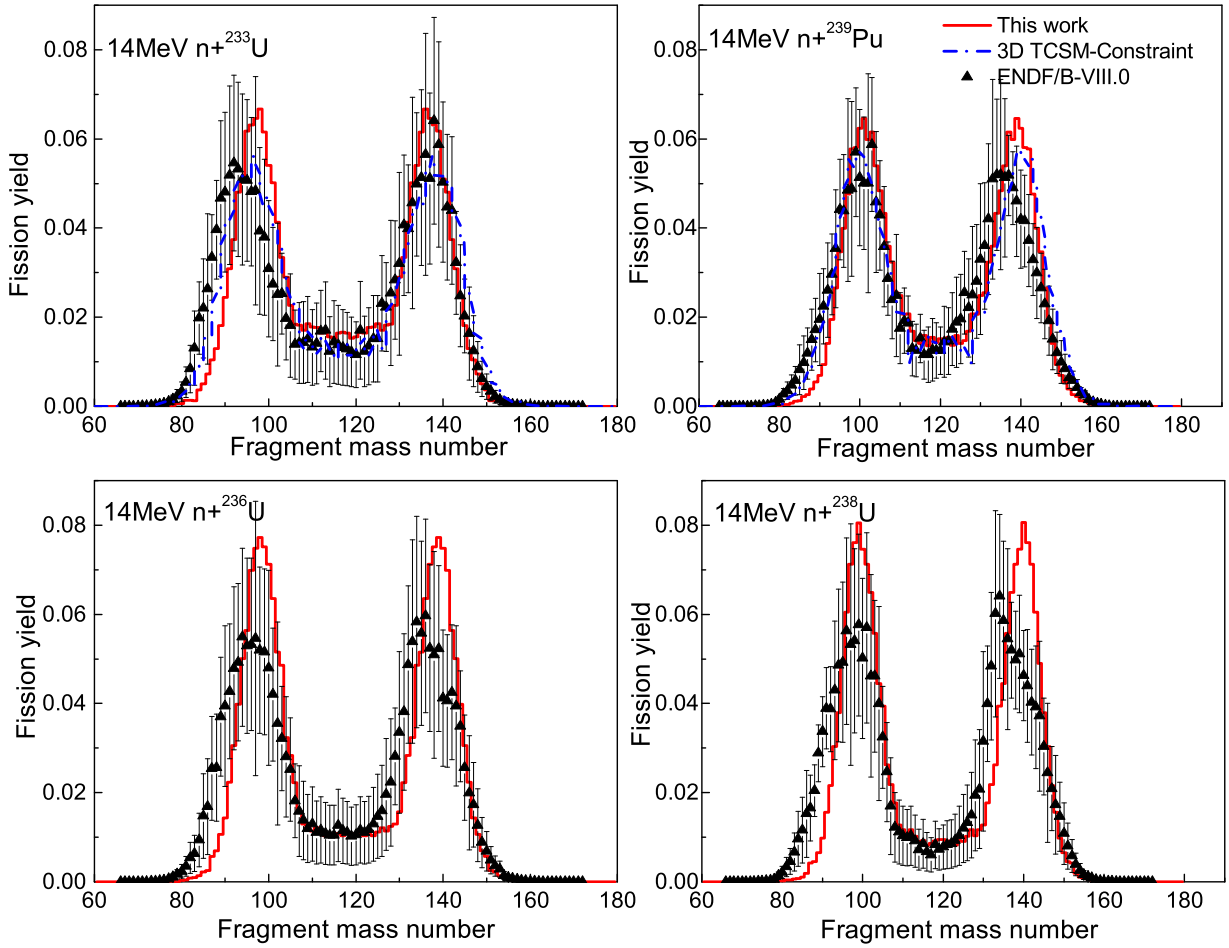

FIG. 8. The calculated fragment mass distributions in 14 MeV $n + {}^{233,236,238}$U and ^{239}Pu fission (red curve) along with the results calculated within the 3D Langevin approach plus a constraint on the heavy fragment deformation based on the TCSM (blue dashed-dot curve) and the evaluated data from ENDF/B-VIII.0.

peak heights are higher, which is possible because the potential energy valley for the asymmetric fission channel is deeper for the odd-*A* fissioning systems.

The calculation results of the TKE as a function of heavy fragment mass for 14 MeV $n + {}^{233}$U and ^{239}Pu fission are presented in Fig. 9, where the comparison with the results of the GEneral description of Fission observables (GEF) code and the experimental data is also shown. It is shown that the calculated TKE results agree well with the experimental data and the GEF results [43] at the large asymmetric mass region. However, there is a large difference among the calculated results of the present work and the GEF and the experimental data at the symmetric mass region, and the TKE of the present work is between the experimental data and the GEF results. The description of the deformation of the fissioning nucleus at the scission point influences the TKE strongly, as discussed in Ref. [14]. The discrepancy shown in Fig. 9 implies the need of improvement of the present model.

Furthermore, the calculated probability distributions of the TKE in 14 MeV $n + {}^{233}$U and ^{239}Pu fission are compared with the results obtained by the GEF model, which is shown at the bottom of Fig. 9. The shapes of the TKE distributions are Gaussian-like ones, while those with GEF deviate from a Gaussian-like distribution in the left side of the distribution. In this work, the mean TKE in 14 MeV $n + {}^{233}$U fission is 168.62 MeV, and the latest experimental data in Ref. [44] is 167.7 MeV, which shows a good agreement between them. And the mean TKE in 14 MeV $n + {}^{239}$Pu fission is 172.99 MeV, which is close to the measured value 175.43 MeV in Ref. [45]. It should be noted that the multichance fission is not taken into account in the present work, which will influence the TKE calculation results.

IV. SUMMARY

In this work, the Langevin approach is extendedly applied to study the dynamical process of nuclear fission within the Fourier shape parametrization, where the potential energy is calculated with the macroscopic-microscopic model based on the Lublin-Strasbourg drop (LSD) model and the Yukawa-folded potential. Within the present model, the calculated fragment mass distributions and the TKE distributions in 14 MeV $n + {}^{233,235,236,238}$U and ^{239}Pu fission are in agreement with experimental data, and the correlation between the deformation parameters at the scission point is studied as well.

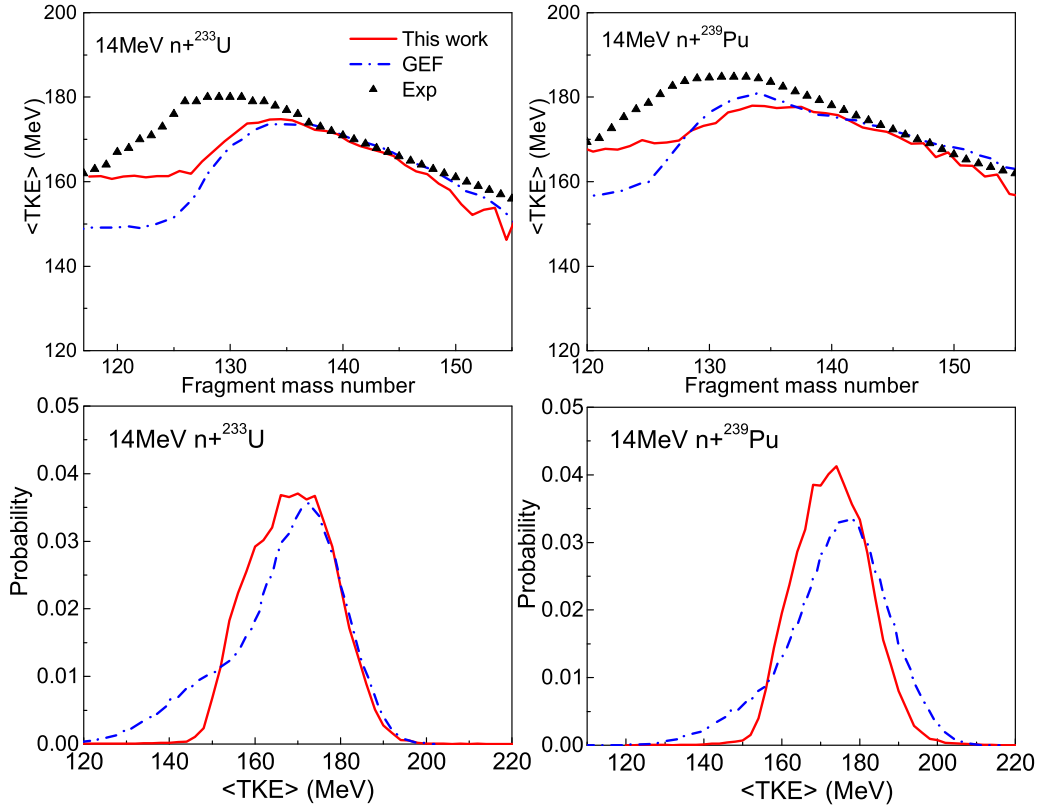

FIG. 9. The calculated total kinetic energy distribution (top) and the probability distribution (bottom) in 14 MeV $n + {}^{233}$U and ^{239}Pu fission, compared with the calculated results with the GEF model and the experimental data [45].

We first investigate the fragment mass and the TKE distributions in 14 MeV $n + {}^{235}$U fission and the results show that the Wall model for the friction tensor is available to describe well both of the mass distribution and the TKE distribution in the nuclear fission, which shows the advantage of the Fourier shape parametrization, *i.e.*, its convenience and validity. Also, the mass-energy correlation of fragments in 14 MeV $n + {}^{235}$U fission is studied, which clearly shows that the asymmetric fission mode dominates among all the fission events and the symmetric fission mode corresponds to the superlong fission.

The correlation of the deformation parameters at the scission point is then studied within the present model. The correlation of the distance between the centers of mass of two fragments R_{12} with the heavy fragment mass is found to be consistent with the TKE as a function of heavy fragment mass and the shortest R_{12} locates around $A_h = 135$ which is due to the influence of the shell effects around the shell closure $Z = 50$ and $N = 82$. The correlation between the R_{12} and the parameter q_2 is also obtained from the dynamical calculation, which indicates that the q_2 introduced in the Fourier parametrization is the optimal elongation parameter.

Last, the present model is adopted to study the mass distributions and the TKE distributions in 14 MeV $n + {}^{233,236,238}$U and ^{239}Pu fission and the overall results agree with the evaluated data and the experimental data. However, the calculated TKE cannot describe the experimental data well around the symmetric mass region, which will be left to the improvement of the model in the future work.

ACKNOWLEDGMENTS

This work was supported by the National Natural Science Foundation of China under Grants No. 11961131010, No. 11790320, No. 11790324, No. 11790325, No. 11790323 and by the Polish National Science Center (Grant No. 2018/30/Q/ST2/00185), and by the Continuous Basic Scientific Research Project (No. WDJC-2019-09).

[1] G. Scamps and C. Simenel, Nature **564**, 382 (2018).
[2] A. Bulgac, P. Magierski, K. J. Roche, and I. Stetcu, Phys. Rev. Lett **116**, 122504 (2016).
[3] N. Schunck, D. Duke, H. Carr, and A. Knoll, Phys. Rev. C **90**, 054305 (2014).
[4] J. A. Maruhn, P. G. Reinhard, P. D. Stevenson, and A. S. Umar, Comput. Phys. Commun. **185**, 2195 (2014).
[5] J. Zhao, T. Nikšić, D. Vretenar, and S.-G. Zhou, Phys. Rev. C **101**, 064605 (2020)

[6] H. Tao, J. Zhao, Z. P. Li, T. Nikšić, and D. Vretenar, Phys. Rev. C **96**, 024319 (2017).
[7] J. C. Pei, W. Nazarewicz, J. A. Sheikh, and A. K. Kerman, Phys. Rev. Lett. **102**, 192501 (2009).
[8] J. Randrup and P. Möller, Phys. Rev. Lett. **106**, 132503 (2011).
[9] A. J. Sierk, Phys. Rev. C **96**, 034603 (2017).
[10] M. R. Mumpower, P. Jaffke, M. Verriere, and J. Randrup, Phys. Rev. C **101**, 054607 (2020).
[11] K. Pomorski, A. Dobrowolski, R. Han, B. Nerlo-Pomorska, M. Warda, Z. Xiao, Y. Chen, L. Liu, and J.-L. Tian, Phys. Rev. C **101**, 064602 (2020)
[12] Y. Aritomo, S. Chiba, and F. Ivanyuk, Phys. Rev. C **90**, 054609 (2014).
[13] M. D. Usang, F. A. Ivanyuk, C. Ishizuka, and S. Chiba, Phys. Rev. C **96**, 064617 (2017).
[14] C. Ishizuka, M. D. Usang, F. A. Ivanyuk, J. A. Maruhn, K. Nishio, and S. Chiba, Phys. Rev. C **96**, 064616 (2017).
[15] M. R. Pahlavani and S. M. Mirfathi, Phys. Rev. C **93**, 044617 (2016)
[16] H. Pasca, A. V. Andreev, G. G. Adamian, N. V. Antonenko, and Y. Kim, Phys. Rev. C **93**, 054602 (2016).
[17] N. Carjan, F. A. Ivanyuk, and Yu. Ts. Oganessian, Phys. Rev. C **99**, 064606 (2019)
[18] T. Asano, T. Wada, M. Ohta, T. Ichikawa, S. Yamaji, and H. Nakahara, J. Nucl. Radiochem. Sci. **5**, 1 (2004).
[19] H. Eslamizadeh and H. Raanaei, Phys. Lett. B **783**, 163 (2018).
[20] L.-L. Liu, X.-Z. Wu, Y.-J. Chen, C.-W. Shen, Z.-X. Li, and Z.-G. Ge, Phys. Rev. C **99**, 044614 (2019).
[21] R. W. Hasse and W. D. Myers, *Geometrical Relationships of Macroscopic Nuclear Physics* (Spinger-Verlag, Berlin, 1988).
[22] J. A. Maruhn and W. Greiner, Z. Phys. **251**, 431 (1972).
[23] A. V. Karpov and V. V. Saiko, Phys. Rev. C **96**, 024618 (2017).
[24] C. Schmitt, K. Pomorski, B. Nerlo-Pomorska, and J. Bartel, Phys. Rev. C **95**, 034612 (2017)
[25] K. Pomorski and J. Dudek, Phys. Rev. C **67**, 044316 (2003).
[26] K. T. R. Davies and J. R. Nix, Phys. Rev. C **14**, 1977 (1976).
[27] A. Dobrowolski, K. Pomorski, and J. Bartel, Comput. Phys. Commun. **199**, 118 (2016).
[28] V. M. Strutinsky, Nucl. Phys. A **95**, 420 (1967).
[29] M. Brack, J. Damgaard, A. S. Jensen, H. C. Pauli, V. M. Strutinsky, and C. Y. Wong, Rev. Mod. Phys. **44**, 320 (1972).
[30] S. G. Nilsson, C. F. Tsang, A. Sobiczewski, Z. Szymański, S. Wycech, C. Gustafson, I.-L. Lamm, P. Möll, and B. Nilsson, Nucl. Phys. A **131**, 1 (1969).
[31] A. V. Ignatyuk, K. K. Istekov, and G. N. Smirenkin, Yad. Fiz. **29**, 895 (1979) [Sov. J. Nucl. Phys. **29**, 450 (1979)].
[32] J. Randrup and P. Moller, Phys. Rev. C **88**, 064606 (2013).
[33] K. T. R. Davies, A. J. Sierk, and J. R. Nix, Phys. Rev. C **13**, 2385 (1976).
[34] J. Blocki, Y. Boneh, J. R. Nix, J. Randrup, M. Robel, A. J. Sierk, and W. J. Swiatecki, Ann. Phys. (NY) **113**, 330 (1978).
[35] H. Feldmeier, Rep. Prog. Phys. **50**, 915 (1987).
[36] H. J. Krappe and K. Pomorski, *Theory of Nuclear Fission: A Textbook, Lecture Notes in Physics* (Springer, Berlin, 2012), Vol. 838.
[37] J. Bartel, B. Nerlo-Pomorska, K. Pomorski, and A. Dobrowolski, Comput. Phys. Commun. **241**, 139 (2019).
[38] H. Hofmann, C. Grégoire, R. Lucas, and C. Ngô, Z. Phys. A **293**, 229 (1979).
[39] H. Hofmann and D. Kiderlen, Int. J. Mod. Phys. E **07**, 243 (1998).
[40] D. A. Brown *et al.*, Nucl. Data Sheets **148**, 1 (2018).
[41] P. P. Dyachenko and B. D. Kuzminov, Yad. Fiz. **7**, 36 (1968) [Sov. J. Nucl. Phys. **7**, 27 (1968)].
[42] P. P. Dyachenko, B. D. Kuzminov, and M. Z. Tarasko, Sov. J. Nucl. Phys. **8**, 165 (1969).
[43] K.-H. Schmidt, B. Jurado, C. Amouroux, and C. Schmitt, Nucl. Data Sheets **131**, 107 (2016).
[44] D. Higgins, U. Greife, F. Tovesson, B. Manning, D. Mayorov, S. Mosby, and K. Schmitt, Phys. Rev. C **101**, 014601 (2020).
[45] V. M. Surin, A. I. Sergachev, N. I. Rezchikov, and B. D. Kuzminov, Sov. J. Nucl. Phys. **14**, 523 (1972).